

Self-Similar Evolution of Gravitational Clustering II: N-Body Simulations of the $n = -2$ Spectrum

Bhuvnesh Jain¹ and Edmund Bertschinger²

¹Department of Physics & Astronomy, Johns Hopkins University, Baltimore, MD 21218.

Email: bjain@pha.jhu.edu

²Department of Physics, MIT, Cambridge, MA 02139. Email: edbert@arcturus.mit.edu

ABSTRACT

The power spectrum $P(k) \propto k^n$ with $n = -2$ is close to the shape of the measured galaxy spectrum on small scales. Unfortunately this spectrum has proven rather difficult to simulate. Further, 2-dimensional simulations have suggested a breakdown of self-similar scaling for spectra with $n < -1$ due to divergent contributions from the coupling of long wave modes. This paper is the second (numerical) part of our investigation into nonlinear gravitational clustering of scale-free spectra, in particular to test the scaling of the $n = -2$ spectrum.

Using high-resolution N-body simulations we find that the $n = -2$ power spectrum displays self-similar scaling. The phase shift of Fourier modes of the density show a dual scaling, self-similar scaling at early times and a scaling driven by the bulk velocity at late times. The second scaling was shown analytically to be a kinematical effect which does not affect the growth of clustering. Thus our analytical and N-body results verify that self-similarity in gravitational clustering holds for $-3 < n < 1$. The N-body spectrum is also compared with analytic fitting formulae, which are found to slightly underestimate the power in the nonlinear regime. The asymptotic shape of the spectrum at high- k is a power law with the same slope as predicted by the stable clustering hypothesis.

Subject headings: cosmology: theory — large-scale structure of universe — galaxies: clustering — galaxies: formation

1. Introduction

The self-similar scaling of density perturbations with scale free initial conditions in a spatially flat universe is a useful theoretical tool in studying structure formation. It has been widely used to study gravitational clustering in cosmology and has been tested by several studies using N-body simulations. However self-similar scaling for scale free initial spectra $P_{\text{lin}}(k) \propto k^n$ has not been adequately demonstrated for $n < -1$ because the requirements of dynamic range get increasingly difficult to meet as n gets smaller. Indeed results of some two dimensional studies suggest a breaking of self-similar scaling for $n = -2$ in three dimensions. Analytical analyses have been limited to the observation that the linear peculiar velocity field diverges for $n < -1$, but the linear density contrast does not diverge provided $n > -3$. This would suggest that while there may be formal problems with establishing self-similarity for $n < -1$, in practice it should hold as long as $n > -3$.

In an earlier paper (Jain & Bertschinger 1996 – Paper I), we have analyzed the dynamics of the coupling of long wave modes by analytical techniques to address the question of whether self-similar scaling is broken for $n < -1$. On the basis of the nonlinear growth of density perturbations we concluded that self-similar scaling does not break down provided $n > -3$, consistent with the linear theory expectation. We also identified statistical measures which would scale differently from self-similar scaling owing to the kinematic effect of large-scale bulk flows. These measures are related to the phase of the Fourier space density field, but do not affect the growth of its amplitude.

In this paper we examine the scaling behavior of the $n = -2$ spectrum using high resolution three dimensional N-body simulations. Testing self-similarity using simulations is crucial because the analytical demonstration of a scale-free dynamics provides no guarantee that the similarity solution will actually hold, starting from some general initial conditions. Moreover, the analytical results of Paper I relied on an assumption about the initial fields, as well as on using the fluid limit approximation. The N-body simulations do not rely on these approximations, though as we shall see their finite resolution introduces other departures from exact self-similarity. Hence by combining our analytical and numerical results, we attempt to provide a complete analysis of the scaling behavior of scale free spectra for $-3 < n < 1$.

We shall consider the similarity properties of gravitational dynamics in a zero-pressure Einstein-de Sitter cosmology. An Einstein-de Sitter universe refers to the model with the cosmological density parameter $\Omega = \Omega_{\text{matter}} = 1$ and zero cosmological constant, so that the universe is spatially flat. The gravitational interaction also does not pick a special length scale. Further let the initial power spectrum be a power law, $P_{\text{lin}}(k) \propto k^n$, over length scales of interest. In such a case there is no preferred length scale in the universe, and the evolution of structure is expected to be self-similar in time.

The resulting self-similar scaling of characteristic length scales x , and wavenumber scales k is (Peebles 1980, Section 73):

$$x_{ss}(t) \propto a(t)^{2/(3+n)} \quad ; \quad k_{ss}(t) \sim x_{ss}(t)^{-1} \propto a(t)^{-2/(3+n)}, \quad (1)$$

where $a(t)$ is the expansion scale factor. The above scaling is most simply derived by requiring consistency with the growth of the rms linear density contrast, smoothed on a scale $x_{ss} = k_{ss}^{-1}$, and related to the power spectrum as:

$$\left(\frac{\delta\rho}{\rho}\right)^2(x_{ss}, t) = \int d^3k a^2 P_{\text{lin}}(k) W^2(kx_{ss}) \simeq 4\pi a^2 k_{ss}^{3+n}, \quad (2)$$

where $W(kx)$ is the smoothing window function. Requiring that the scale at which $(\delta\rho/\rho) = 1$ scales self-similarly gives the result in equation (1).

Early studies of self-similar evolution in cosmology include those of Peebles (1974); Press & Schechter (1974); Davis & Peebles (1977); and Efstathiou & Eastwood (1981). Efstathiou et al. (1988) tested self-similar scaling in N-body simulations of scale free spectra with $n = -2, -1, 0, 1$. They examined the scaling of the correlation function $\xi(x, t)$, and of the multiplicity function describing the distribution of bound objects. They verified the predicted scaling for both statistics, and found consistency with the picture of hierarchical formation of nonlinear structure on increasingly large length scales. Their results for $n = -2$ did not match with the self-similar scaling as well as the other cases. Bertschinger & Gelb (1991) used better resolution simulations to address these questions and also found similar results. These authors concluded that the reason for the weakness of the $n = -2$ results was the finite size of their simulation box, as the $n = -2$ case has more power on large scales and therefore requires a larger box-size to approximate the infinite volume limit with the same accuracy as larger values of n .

More recently Lacey & Cole (1994) have examined the self-similar scaling of the number density of nonlinear clumps for scale-free spectra. Their results indicate that self-similar scaling works reasonably well for the statistics they measure, even for $n = -2$. Jain, Mo & White (1995) and Padmanabhan et al. (1995) reach the same conclusion for the correlation function and power spectrum. Colombi, Bouchet & Hernquist (1995) have verified self-similarity for higher moments of the density. However, in all the above studies the self-similar scaling of a particular statistic is tested without making a comparison with alternate scalings. As demonstrated in Section 4, this makes it difficult to distinguish the effect of limited numerical resolution from a real breakdown of self-similar scaling.

The N-body results of Ryden & Gramann (1991), and Gramann (1992) suggest that the $n = -2$ case is different from $n \geq -1$ for a fundamental reason. They studied $n = -1$

simulations in two dimensions, which are the analog of $n = -2$ in three dimensions, and examined the scaling of the phase (Ryden & Gramann 1991), and then both phase and amplitude (Gramann 1992) of the Fourier transform of the density field. The scaling was found to be different from the standard self-similar scaling. Characteristic wavenumber scales, instead of following the self-similar scaling, given in two dimensions by $k_{ss}(t) \propto a(t)^{-2/(2+n)} \propto a(t)^{-2}$, showed the scaling $k \propto a(t)^{-1}$. Other studies in two dimensions also suggest that a transition in nonlinear evolution occurs at $n = -1$ (Klypin & Melott 1992, and references therein). Motivated by Gramann’s results we had re-examined the $n = -2$ simulation presented in Bertschinger & Gelb (1991) and found that the results were ambiguous, and that a bigger simulation would be needed to provide a definitive answer.

In this paper we use the $n = -2$ case as representative of the range $-3 < n < -1$ and use high resolution N-body simulations to test for self-similar scaling. Section 2 provides the analytical background and motivates the need to test the scaling of spectra with $n < -1$. The N-body simulations used to test self-similar scaling are described in Section 3, and effects of finite numerical resolution are discussed. In Section 4 results for the scaling of the power spectrum are presented and self-similar scaling is compared with an alternate scaling. In Section 5 a different statistic is used which measures the scaling of the amplitude as well as the phase of the Fourier space density. We discuss subtleties in measuring the evolution of the phase, and provide a kinematical interpretation of the results for the phase shift. We conclude in Section 6 by discussing the results of this paper and Paper I.

2. Analytical Background

This section summarizes the formalism and motivation presented in Section 2 of Paper I. We use comoving coordinates \vec{x} and conformal time $d\tau = dt/a(t)$ to write the nonrelativistic cosmological fluid equations as

$$\frac{\partial \delta}{\partial \tau} + \vec{\nabla} \cdot [(1 + \delta)\vec{v}] = 0 , \quad (3a)$$

$$\frac{\partial \vec{v}}{\partial \tau} + (\vec{v} \cdot \vec{\nabla}) \vec{v} = -\frac{\dot{a}}{a} \vec{v} - \vec{\nabla} \phi , \quad (3b)$$

$$\nabla^2 \phi = 4\pi G a^2 \bar{\rho} \delta , \quad (3c)$$

where $\dot{a} \equiv da/d\tau$, $\delta(\vec{x}, \tau) = (\rho(\vec{x}, \tau) - \bar{\rho}(\tau))/\bar{\rho}(\tau)$, $\phi(\vec{x}, \tau)$ is the perturbed gravitational potential, and $\vec{v}(\vec{x}, \tau) \equiv d\vec{x}/d\tau$ is the proper peculiar velocity. We assume an Einstein-de

Sitter ($\Omega = 1$) universe, with $a \propto t^{2/3} \propto \tau^2$. We will also assume that the initial (linear) density fluctuation field is a Gaussian random field.

The fluid equations (3) are strictly valid only on scales large compared to the nonlinear clustering scale. On scales much smaller than the nonlinear scale, the intersection of particle trajectories leads to a complicated, anisotropic stress tensor and thus invalidates a fluid description which requires the density and velocity to be smooth, single-valued functions of position. Whereas the analytical analysis of Paper I used the zero-pressure fluid approximation and the continuum limit, the N-body simulations do not as they integrate the equations of motion for the particle trajectories.

To quantify the amplitude of fluctuations on various scales it is preferable to work with the Fourier transform of the density fluctuation field, which we define as

$$\hat{\delta}(\vec{k}, \tau) = \int \frac{d^3x}{(2\pi)^3} e^{-i\vec{k}\cdot\vec{x}} \delta(\vec{x}, \tau). \quad (4)$$

The power spectrum (power spectral density) of $\delta(\vec{x}, \tau)$ is defined by the ensemble average two-point function,

$$\langle \hat{\delta}(\vec{k}_1, \tau) \hat{\delta}(\vec{k}_2, \tau) \rangle = P(k_1, \tau) \delta_{\text{D}}(\vec{k}_1 + \vec{k}_2), \quad (5)$$

where δ_{D} is the Dirac delta function, required for a spatially homogeneous random density field. For a homogeneous and isotropic random field the power spectrum depends only on the magnitude of the wavevector. The contribution to the variance of $\delta(\vec{x}, \tau)$ from waves in the wavevector volume element d^3k is $P(k, \tau)d^3k$. The autocorrelation function is defined as $\xi(x, \tau) = \langle \delta(\vec{x}_1, \tau)\delta(\vec{x}_2, \tau) \rangle$, where $|\vec{x}_1 - \vec{x}_2| = x$. It can be easily verified that $\xi(x, \tau)$ is the Fourier transform of $P(k, \tau)$.

The analytical approach developed in Paper I can now be summarized as follows. For a scale free initial spectrum $P_{\text{lin}}(k) \propto k^n$, the rms density contrast in linear theory is given by equation (2). As $k \rightarrow 0$ the window function generically (e.g. the top-hat or Gaussian window functions) has the limiting form $W(kx) \rightarrow 1$. Hence for $n \leq -3$ the linear rms density contrast on any scale receives divergent contributions from the $k \rightarrow 0$ part of the spectrum. Analogous to the rms density contrast one can define the bulk flow velocity, which is the average, smoothed peculiar velocity on scale x . It is obtained by using the peculiar velocity power spectrum $P_{\text{lin}v}$ in equation (2) instead of P_{lin} . From equation (3a) it follows that $\dot{\delta} = -\vec{\nabla} \cdot \vec{v}$ in linear theory, or $P_{\text{lin}v}(k) = \dot{a}^2/a^2 P_{\text{lin}}(k)/k^2$. Thus the bulk velocity is given by

$$v_b^2(x, \tau) = \dot{a}^2 4\pi \int dk P_{\text{lin}}(k) W^2(kx). \quad (6)$$

For $n < -1$, $v_b(x, \tau)$ diverges due to the $k \rightarrow 0$ contribution. Since the nonlinear fluid equations couple the density and velocity, this divergence manifests itself in the nonlinear

terms in the fluid equations.

If this divergence were to have a dynamical influence in the growth of the density contrast it would lead to a breakdown of self-similar scaling, because it introduces a new scale in the system. Setting $v_b(x) = \text{constant} \leq c$, with a finite lower limit in the integral in equation (6) gives the scaling $x \propto a$ for all $n < -1$. The standard self-similar scaling of equation (1) then holds only if $n > -1$. This, coupled with the numerical results of Gramann (1992) described in Section 1, provided the motivation for our analytical examination of spectra with $n < -1$ in Paper I. The results of Paper I are summarized in Section 5. In the following sections we will analyze the scaling of the $n = -2$ spectrum in N-body simulations to test whether it follows the velocity scaling $x \propto a$ or the self-similar scaling of equation (1): $x \propto a^2$.

3. The N-body Simulations

N-body simulations provide a powerful means for testing the self-similar scaling of scale free spectra. The deeply nonlinear regime is accessible in these simulations, thus offering the possibility of measuring the complete similarity solution. N-body simulations have limited dynamic range, but they do not rely on any approximations of the kind made in Paper I. Since the equations of motion for individual particles are integrated, the fluid limit approximation is not required either. Therefore they provide a complementary technique to the analytic approaches of Paper I.

The simulations used for the self-similar scaling analysis are three dimensional particle-particle/particle-mesh (P³M) simulations. The larger of our $n = -2$ simulations had 256^3 particles and a Plummer force softening parameter $\epsilon = 1/5120 L$, where L is the box-length. It was performed on the CM-5 supercomputer at the National Center for Supercomputing Applications using the parallel code of Ferrell & Bertschinger (1994, 1995). This simulation, labeled A in Table 1, is used for the main results of this paper. To test the effects of numerical resolution at high- k we have compared the results with a smaller P³M simulation (labeled B), performed on a workstation, which used half as many particles and twice the force softening length. This simulation used a variable PM mesh as shown in table 1. We have also used a set of three PM simulations (labeled C), performed on the CM-5, to estimate the effects of statistical fluctuations at low- k . Table 1 gives the relevant parameters of all the simulations used.

The initial positions and velocities for the particles were generated using the Zel'dovich approximation, and assumed the linear power spectrum and Gaussian statistics. Outputs

of the particle positions were stored at time intervals corresponding to an increase of a by a factor of $2^{1/4}$. Energy conservation was better than 10^{-4} of the total gravitational energy at all times for simulation A and was similar for the other simulations.

At each of these output times the particle positions were interpolated onto a 1024^3 grid using the triangular-shaped-cloud (TSC) scheme (see Gelb & Bertschinger 1994 for details) to get the real space density. The density field $\delta(\vec{x}, a)$ was then fast Fourier transformed to get $\hat{\delta}(\vec{k}, a)$. $\hat{\delta}(\vec{k}, a)$ is a complex number at each \vec{k} , and is therefore represented by a real and imaginary part. The values of \vec{k} are represented by a three dimensional vector (k_x, k_y, k_z) , with each of k_x, k_y and k_z being integers ranging from -511 to 512 . In the remainder of this section the magnitude of \vec{k} will be given in units of $2\pi/L$, so that the modes with wavelength equal to L have $k = 1$. The power spectrum was computed as the mean of $|\hat{\delta}(\vec{k}, a)|^2$ in bins of k with width $\delta k = 1$. The power spectrum was corrected for the effects of shot noise and of convolution with the TSC interpolating window used to compute the real space density. Figure 1 shows the power spectrum for simulation A at five different values of a , corresponding to values of the nonlinear wavenumber (defined in equation (7) below) $k_{nl}(a) = 58, 29, 14.5, 7.25$. Also shown as the dotted line is the linear spectrum at the same times.

In an N-body simulation there are many departures from the idealization of an infinite, continuous fluid. The limitations common to any N-body simulation are the finite size of the box and the discrete nature of particles. Additional scales are introduced due to the PM mesh, force softening and the density interpolation grid. As discussed in Section 1 of Paper I, the presence of these scales is not a fundamental drawback; it only means that one must be careful to ensure that the range of scales used to study the scaling in time is sufficient to allow for intermediate asymptotic self-similarity to set in. In the following discussion we shall focus on the largest of our simulations, labeled A in Table 1.

An important scale that we shall refer to is the nonlinear scale, at which the fluctuation amplitude is ~ 1 . We define a nonlinear wavenumber as:

$$\int_0^{k_{nl}} d^3k P_{\text{lin}}(a, k) = 1. \quad (7)$$

Table 1: Parameters of the N-body simulations

Simulation	$k_{nl}/(2\pi/L)$	N_{part}	Softening ϵ/L	PM Mesh	Timesteps
A: $n = -2$, P ³ M	5250 – 7.25	256^3	1/5120	512^3	1331
B: $n = -2$, P ³ M	2060 – 4.02	128^3	1/2560	$256^3 - 432^3$	1007
C: $n = -2$, PM	5250 – 7.25	256^3	—	512^3	692

For $P_{\text{lin}}(a, k) = Aa^2k^{-2}$, equation (7) gives $k_{nl}(a) = (4\pi Aa^2)^{-1}$. Thus $k_{nl}(a)$ becomes smaller at late times since the nonlinear length scale increases with time. For scale free spectra $k_{nl}(a)$ provides a useful time variable, for example, in comparing simulations with different starting amplitudes. We now turn to the main numerical limitations in our simulations.

(i) *Initial amplitude.* The initial amplitude used in our $n = -2$ simulations A and C is such that at $a = 1$ the dimensionless power on the Nyquist frequency of the particle grid, $k = 128$ is $4\pi k^3 P(k) = 0.024$. This corresponds to having $k_{nl} = 5250$ at the initial time. The $n = -2$ spectrum needs to be started with very small initial amplitude in order for clustering on small scales to develop self-similarly. As pointed out by Lacey & Cole (1994) the standard prescription of Efstathiou et al. (1985) of having power on the Nyquist frequency of the particle grid equal to the white noise level is too large and produces significant departures from self-similar evolution.

(ii) *Force softening.* Force softening is implemented in computing short range forces in the particle-particle part of the P³M simulations by using the Plummer force law: $F(r) = Gm^2/(r^2 + \epsilon^2)$. The parameter ϵ is given in Table 1 for the various P³M simulations. The distance at which $r^2 F/(Gm^2) = 1/2$ is $\simeq 1.3\epsilon$. This distance is $\simeq L/4000$ for simulation A: it is smaller by almost a factor of 4 than the main limiting factor on small scales, the spacing of the 1024^3 grid used for interpolating the density (as shown below in point (iii), the grid effects are in fact significant up to twice the grid spacing). This is important, since the force softening affects the dynamical evolution and can therefore artificially suppress the clustering on scales several times larger than ϵ . In addition, the finite number of particles and the finite size of the timesteps used limit the numerical resolution on small scales. For the parameters in our simulations these affect the spectrum on about the same limiting scale as the force softening. Hence their effect is also far less important than that of the FFT grid, aside from the PM simulations whose force softening was relatively large.

(iii) *FFT grid.* The density field was fast Fourier transformed to get $\hat{\delta}(\vec{k})$. This involves interpolation on to a grid to get the real space density field, and thus imposes a minimum length scale below which power cannot be measured. Figure 2 shows a comparison of the power spectrum computed for simulation B using two different grid sizes: 512^3 and 1024^3 . Both spectra have been corrected for the effects of convolution with the TSC window. It shows that the power for k up to 1/2 the Nyquist frequency of the FFT grid is accurate to better than 20%. However this is only a consistency check, as a conservative estimate, we therefore use a maximum $k = 256$ for the 1024^3 interpolation and FFT grid in our self-similarity analysis.

(iv) *Statistical fluctuations at low- k .* At low wavenumbers the finite number of modes

present in a given bin in k causes statistical fluctuations in the power spectrum. This is evident in Figure 1 which shows that at $k = 1$ and 2 there are significant differences between $P(k)$ and $P_{\text{lin}}(k)$ even at early times. By checking the power spectra of the three different PM runs of simulation C we found that as the simulation evolved the power in realizations with lower initial power at $k = 1$ and 2 was suppressed out to $k \simeq 5$ due to nonlinear mode coupling. For the latest time output used in our analysis, at $k \geq 5$ these fluctuations are smaller than 20%. For the results shown in Section 4 we plot the power spectra from $k = 3 - 256$.

(v) *Range of $k_{nl}(a)$.* At late times the nonlinear wavenumber $k_{nl}(a)$ approaches the size of the box. This sets a maximum value of a beyond which the absence of modes with wavelength larger than the box-size inhibits the growth of the spectrum at late times, because the coupling of these modes would have enhanced the power at high- k (Jain & Bertschinger 1994). To test this effect, simulation B was evolved to a maximum a corresponding to $k_{nl} = 2$. Using this simulation we find that for the $n = -2$ spectrum the power at $k \lesssim 10$ is indeed underestimated for $k_{nl}(a) \lesssim 4$. At later times, for example with $k_{nl}(a) = 2.8$, the power spectrum at k extending up to $k \simeq 100$ is significantly suppressed relative to the amplitude required to satisfy self-similarity. This problem is particularly severe for the $n = -2$ spectrum because of the large amount of power on low- k relative to spectra with larger n , which in turns leads to a stronger nonlinear coupling with high- k modes. It is the principal reason for the requirement of a large dynamic range to test the scaling properties of this spectrum.

Our choice of $k_{nl}(a_{max}) = 7.25$ for simulation A is adequate to get dynamically accurate power spectra at low- k , and also provides a sufficient range in a to test self-similar evolution. At small a we are limited by the fact that the shot noise amplitude which we subtract from the measured power spectrum exceeds the measured spectrum at high- k for $a < 8$ ($k_{nl} = 82$). This determines the earliest output used in our analysis – for simulation A this had $k_{nl}(a_{min}) = 58$.

(vi) *Accuracy of PM simulations.* A final point, regarding the adequacy of PM simulations to follow the scaling of the $n = -2$ spectrum is made in Figure 3, where the power spectrum of the P³M simulation A is compared with the PM simulation C. These simulations have identical number of particles, the same initial Fourier modes, and are started with the same $k_{nl}(a)$. Both spectra are plotted upto 1/2 the Nyquist frequency of the FFT grid, and can therefore be legitimately compared over the full range of k for which they overlap. The figure shows that at late times the power in the PM simulation is suppressed at wavenumbers significantly smaller than the Nyquist frequency of the PM grid, $k = 512$. At the last output time shown, corresponding to $k_{nl}(a) = 7.25$, the power

at $k > 50$ is suppressed by $> 20\%$. The suppression increases to $> 50\%$ at $k > 80$, i.e. at $k > 1/6$ th the Nyquist frequency of the PM grid. Thus the commonly cited limit of the spatial resolution of PM simulations as being less than twice the grid spacing considerably overestimates the spatial resolution. Our results are at odds with previous tests of PM simulations in the literature (e.g. Splinter, Melott & Shandarin 1997). The difference in these tests is the statistical measures used as well as the degree of nonlinearity, since the discrepancy appears to occur only in the regime of very high over-densities (the last output time shown).

4. Scaling of the Power Spectrum

The self-similar solution for the power spectrum and autocorrelation function is (Peebles 1980, Section 73),

$$P(k, \tau) = a^{3\alpha} k_0^{-3} \hat{P}(ka^\alpha/k_0) ; \xi(x, \tau) = \hat{\xi}(x/x_0 a^\alpha), \quad (8)$$

where $\alpha = 2/(3 + n)$; k_0, x_0 are constants which must be determined from the initial conditions; and $\hat{P}, \hat{\xi}$ are unspecified dimensionless functions. It is easy to verify that the linear spectrum $P_{\text{lin}}(k, \tau) \propto a^2 k^n$ is consistent with the functional form of equation (8). This functional form provides a strong constraint on the evolution of the spectrum, as P is no longer an arbitrary function of two independent variables k and a , but only of the variable ka^α .

The results for the scaling of the power spectrum are shown in Figures 4 and 5. The self-similar scaling given by equation (8) with $n = -2$ is compared with the velocity scaling. The two scalings are distinguished by the way in which characteristic wavenumbers k_c scale with time: $k_c \propto a^{-\alpha}$, with $\alpha = 2$ for self-similar scaling, and $\alpha = 1$ for the velocity scaling, as discussed at the end of Section 2. In Figure 4 we show the measured power spectrum at eight different times corresponding to a range of $k_{nl}(a) = 58 - 7.25$ (in units of $2\pi/L$). Also shown as the dotted curves is the power spectrum from the fourth from last time, re-scaled self-similarly in the left panel, and according to the velocity scaling in the right panel. The results show that the measured spectra are consistent with self-similar scaling and show departures from the velocity scaling which causes the spectrum to grow too slowly at high- k . It should be noted that there are apparent departures from self-similar scaling at low- k . We believe these arise due to the statistical fluctuations resulting from the small number of modes present in the low- k bins. These can be seen even in figure 1 where the power at the lowest k does not agree with the linear spectrum. At the latest times however

this discrepancy extends to $k \simeq 10$. A possible explanation is the missing power from long-wave modes, which, as one might expect from the action of nonlinear mode coupling, appears to affect the spectrum at increasing k at later time outputs. However this issue merits further exploration as it contradicts our own estimate of $k > 4$ being an adequate cut-off at the low- k end.

Figure 5 shows the same feature in a slightly different way: the power spectrum curves at the eight different times are re-scaled so that they would lie along a single curve if they followed the predicted scaling. Again, the left panel which uses self-similar scaling shows that the curves almost coincide. The right panel showing the velocity scaling has significant differences between the different curves even at intermediate k on which the spectrum is measured very accurately. In figures 4 and 5 the agreement with the self-similarly scaled spectra is typically within 20%, and better than 40% over nearly the entire range (excluding only the lowest k where fluctuations occur due to the small number of modes). For the velocity scaling, the agreement is typically at the 50% level and is about a factor of 2 if one uses the earliest and latest output times. The curve traced out by the scaled N-body spectra in the left-panel of figure 5 give the empirical \hat{P} of equation (8).

To highlight the numerical difficulty of demonstrating self-similar scaling for the $n = -2$ spectrum, in Figure 6 we show the results from the smaller of our P³M simulations, labeled B in Table 1. The figure shows the scaling of the spectrum in exactly the same way as Figure 5. On comparing the two panels in Figure 6 it is evident that the dynamic range of simulation B is not adequate to discriminate between the self-similar and velocity scalings. The scatter in the different curves due to numerical effects at low and high- k (which overlap with intermediate- k spectra at other times because of the re-scaling made in the plots) is comparable to the difference in the self-similar and velocity scalings. It is also clear that without comparing the two scalings, it is very difficult to distinguish the effects of limited dynamic range from real departures from the underlying scaling.

The resolution of simulation B shown in Figure 6 is comparable to the simulations used by Lacey & Cole (1994) and Jain, Mo & White (1995). Lacey & Cole used a P³M simulation with 128^3 particles and $\epsilon = L/4160$, while the simulation used by Jain, Mo & White was simulation B itself. Colombi, Bouchet & Hernquist (1995) used a treecode simulation with 64^3 particles and a spatial resolution somewhat larger than that of simulation B. The resolution limitations of the PM simulation C are even more severe than those of simulation B. At late times the power at high- k is significantly smaller than that required for self-similarity. As discussed at the end of the previous section, Figure 3 shows that for simulation C the power on $k > 80$, i.e. on k larger than 1/6th the Nyquist frequency of the PM grid, is artificially suppressed by 50% at the latest a with $k_{nl}(a) = 7.25$ (in units

of $2\pi/L$). The $n = -2$ simulation of Padmanabhan et al. (1995) is a PM simulation with 240^3 particles on a 720^3 PM mesh, and used a staggered mesh scheme. Thus its spatial resolution is about twice superior to that of simulation C, but is still considerably worse than that of simulation B (since its PM grid spacing is $> 2\epsilon$ for simulation B) which is shown in Figure 6 to lack the resolution to test self-similar scaling.

4.1. Shape of the Nonlinear Spectrum

Having shown that simulation A for the $n = -2$ spectrum follows self-similar scaling, we can characterize the spectrum at any time by the self-similar functional form of equation (8). The qualitative features of this shape can be seen in Figure 1 which shows the nonlinear and linear $P(a, k)$ at five different times, and in Figure 5 which shows the self-similar shape of the spectrum traced out by the measured spectra at eight different times. At sufficiently low (k/k_{nl}) the spectrum follows the linear shape $\propto k^{-2}$. At $k \sim k_{nl}$ the spectrum rises above the linear spectrum and then at still higher k it again approaches the shape $\propto k^{-2}$. The enhancement of the nonlinear spectrum relative to the linear spectrum is a factor of $\simeq 1.5$ at $k = k_{nl}$, and approaches a factor $\simeq 5$ at $k \gtrsim 10 k_{nl}$. It maintains this enhancement up to the highest k measured.

The shape of $P(k)$ measured at $k \gtrsim 10 k_{nl}$ is in agreement with the prediction of the stable clustering ansatz. This ansatz relies on the assumption that the mean pair velocity in physical coordinates is zero. As shown by Davis & Peebles (1977) this leads to the prediction that the asymptotic form of $P(k)$ at high- k is: $P(a, k) \propto a^{6/(5+n)} k^{-6/(5+n)}$. For $n = -2$ this is: $P \propto a^2 k^{-2}$, in excellent agreement with the measured slope shown in Figure 5. Note that once self-similarity is taken to be valid, the growth in a is fixed by the k^{-2} shape. Note also that for $n = -2$ the shape of the spectrum in the stable clustering regime is the same as that of the linear spectrum.

The transition from the linear regime to the deeply nonlinear regime of stable clustering is poorly understood analytically, since perturbation theory breaks down at $k \sim k_{nl}$. However a semi-empirical prescription for obtaining the nonlinear ξ for arbitrary initial spectra was proposed by Hamilton et al. (1991), and extended to the power spectrum by Peacock & Dodds (1994). Jain, Mo & White (1995) and Peacock & Dodds (1996) have refined the prescription to take into account a dependence on the initial spectrum. They provide fitting formulae for the dimensionless nonlinear spectrum at a given time, $\Delta(a, k) = 4\pi k^3 P(a, k)$ in terms of the linear spectrum $\Delta_L(a, k_L) = 4\pi k^3 P_{\text{lin}}(a, k_L)$ evaluated at a smaller wavenumber k_L as indicated. The two wavenumbers k_L and k are related by

$k = [1 + \Delta(k)]^{1/3} k_L$. One has to first obtain $\Delta(k)$ for given k_L and Δ_L using equation 9 below, and then substitute it into the relation above to get the value of k . The relation between $\Delta(a, k)$ and $\Delta_L(a, k_L)$ is (Jain, Mo & White 1995):

$$\frac{\Delta(a, k)}{B(n)} = \Phi \left[\frac{\Delta_L(a, k_L)}{B(n)} \right], \quad (9)$$

where the constant $B(n) = [(3 + n)/3]^{1.3}$, and the function Φ is

$$\Phi(x) = x \left(\frac{1 + 0.6x + x^2 - 0.2x^3 - 1.5x^{7/2} + x^4}{1 + 0.0037x^3} \right)^{1/2}. \quad (10)$$

The formulae proposed by Peacock & Dodds (1996) give similar results as the equations above, though the nonlinear asymptote is somewhat lower for the $n = -2$ spectrum.

The fitting formula given above can be tested by using the nonlinear spectrum measured in our simulations. The results for the spectrum from simulation A are shown in Figure 7. The dimensionless spectrum $\Delta(a, k)$ is plotted against $\Delta_L(a, k_L)$ for the output times shown in Figure 1. The solid curve shows the fit provided by equations (9) and (10). The dashed curve is obtained from the fitting formula of Peacock & Dodds (1996). The dotted lines show the slope of the linear and stable clustering predictions. The agreement between the N-body spectra and the solid curve is adequate, and is better than about 30% over almost the entire range plotted (note that the accuracy of the N-body spectrum at the smallest and largest amplitudes shown is about 20%). The N-body spectrum is enhanced relative to the fit at large amplitudes. This is in the same sense as the discrepancy noted by Jain, Mo & White (1995) who observed that the $n = -2$ spectrum has a slightly steeper nonlinear shape in the $\Delta(k) - \Delta_L(k_L)$ plot as compared to spectra with larger n . The results also show that the N-body spectra approach the stable clustering slope at amplitudes of $\Delta(k) \gtrsim 50$.

5. Alternate Measures of Scaling

The scaling properties of the matter distribution for scale-free conditions can be measured from any appropriate statistical measure. The power spectrum is the second moment of the density field, and is therefore one such statistic. The previous section demonstrated that it is only with very large simulation that the scaling of the power spectrum can be accurately tested. Higher order statistics are even harder to measure accurately. Of course every statistical measure which relates to the growth of perturbations

should measure the same scaling properties, but to measure them in N-body simulations for “difficult” spectra like $n = -2$, it is important to check more than one statistic. In this section we measure the scaling properties of the full density field by using a different approach. Rather than compute a statistic and then measure its scaling in time, we compute the fractional departure of the phase and amplitude from linear evolution mode by mode. The degree of nonlinearity thus measured is used to define characteristic nonlinear scales for the phase and amplitude. Thus by using both the phase and amplitude, and by using the nonlinearity of individual modes rather than an averaged quantity like the power spectrum, we are able to probe the scaling of the full density field more completely.

We use the data for $\hat{\delta}(\vec{k}, a)$ to compute the amplitude Δ and phase ϕ given by,

$$\hat{\delta}(\vec{k}, a) = \Delta(\vec{k}, a)e^{i\phi(\vec{k}, a)}. \quad (11)$$

Δ and ϕ are the basic variables used for the scaling analysis in this section. In Figures 8-10 the trajectories of the phase and amplitude of individual Fourier modes as a function of time are shown for the $n = -2$ simulation. Each of these figures has four panels, and each panel shows the evolution of five modes, chosen so that they represent a large range in k . These figures give an idea of how individual modes evolve, in contrast to the regular behavior shown by the statistics computed from them. Even at relatively early times when most statistics obey linear behavior the amplitudes and phases can be seen to follow quite jagged paths, with the amplitude even showing negative growth for some time intervals. This suggests that there is more information to be mined than is provided by conventional statistics.

5.1. Measuring the Phase Shift

A technical problem in the measurement of the phase arises because conventionally the phases are defined modulo (2π) . The phase trajectories that result are shown in Figure 8, where all the phases lie between $-\pi$ and π . This is how the phases from N-body data have been computed in previous studies (Ryden & Gramann 1991; Scherrer, Melott & Shandarin 1991; Sugimotohara & Suto 1991). However, following the phase trajectories in Figure 8 makes it clear that this will have the effect of randomizing the phases at late times relative to their initial values, even if the actual growth were monotonic. This is because even a small change in the phase, $\delta\phi$, could cause it to be mapped to a value indicating a change of $(2\pi - |\delta\phi|)$.

If the trajectories could be obtained with arbitrarily small increments in a then such artificial mappings could be un-done, and the phases plotted without constraining them between $-\pi$ and π . Since outputs are available only at discrete values of a , there is a two-fold ambiguity in defining the phase. Consider the phase values at two successive a 's for a given \vec{k} : $\phi(\vec{k}, a_j)$ and $\phi(\vec{k}, a_{j+1})$, defined in the usual way to lie between $-\pi$ and π . Let $\delta\phi_j = \phi(\vec{k}, a_{j+1}) - \phi(\vec{k}, a_j)$. An alternate value for the phase at a_{j+1} is $\phi'(\vec{k}, a_{j+1}) = \phi(\vec{k}, a_j) \pm (2\pi - |\delta\phi_j|)$, where the sign is positive if $\delta\phi_j < 0$ and vice versa. To choose between ϕ and ϕ' , we follow the trajectory of each mode, and at each successive value of a , we define the phase by taking the magnitude of the change in phase to be the smaller of $|\delta\phi_j|$ and $(2\pi - |\delta\phi_j|)$. The result is shown in Figure 9. As long as the typical changes in phase at successive times are less than π , this procedure is a reasonable way of extending the range of ϕ . As we shall see, this considerably extends the degree of phase nonlinearity accessible to our analysis.

5.2. Scaling of the Phase and Amplitude

Following Ryden & Gramann (1991) and Gramann (1992), we define the following statistics as a measure of the degree of nonlinear evolution. For the phase we define the mean deviation from the initial phase, $\overline{\delta\phi}(k, a) \equiv \langle |\delta\phi(\vec{k}, a)| \rangle = \langle |\phi(\vec{k}, a) - \phi(\vec{k}, a_i)| \rangle$, where a_i is the initial value of a . The averages indicated are performed over the different modes within a shell in k -space whose wavenumbers lie between $(k - 0.5)$ and $(k + 0.5)$. For the amplitude we simply measure the mean amplitude $\langle \Delta(\vec{k}, a) \rangle$ within each shell in k -space. If we had used the phase trajectories as shown in Figure 8 (i.e., defined to lie between $-\pi$ and π), then at late times $\overline{\delta\phi}(k, a)$ would have reached a maximum value $2\pi/3$ — this corresponds to a distribution of $\phi(\vec{k}, a)$ that is uncorrelated with $\phi(\vec{k}, a_i)$. However, we find that $\overline{\delta\phi}$ shows systematic growth well beyond $2\pi/3$. Thus with the phase information that we have generated, previously unexplored aspects of phase evolution in the deeply nonlinear regime can be addressed.

To analyze self-similar scaling, we define two characteristic wavenumbers. The first, denoted $k_c(a, \phi_c)$, is defined by setting $\overline{\delta\phi}(k, a) = \phi_c$, where ϕ_c is a constant. The second, denoted $k_c(a, \Delta_c)$ is defined using the amplitude as follows:

$$\left\langle \frac{|\Delta(\vec{k}, a) - \Delta_1(\vec{k}, a)|}{\Delta_1(\vec{k}, a)} \right\rangle = \Delta_c, \quad (12)$$

where $\Delta_1(\vec{k}, a)$ is the linear solution for Δ , and Δ_c is a dimensionless constant. Thus $k_c(a, \Delta_c)$ is the wavenumber at which the fractional departure of the amplitude from the

linear solution is Δ_c . These statistics involve summing the magnitudes of the departures from linear behavior for each mode within a given k -shell. Hence they probe the degree of nonlinearity more directly than if a statistic was computed first, and then its departure from the linear solution was calculated.

The analytical prediction for the variance of the phase shift given in Paper I is

$$\left\langle \left[\delta\phi(\vec{k}, \tau) \right]^2 \right\rangle = \frac{4\pi}{3} a(\tau)^2 k^2 \int dk_1 P_{\text{lin}}(k_1). \quad (13)$$

Thus the leading order solution for $\hat{\delta}(\vec{k})$ involves a growing (and, for $n < -1$, divergent) phase shift, but there are no contributions to the amplitude at this order. With some further assumptions we were able to show analytically that the amplitude does not diverge provided $n > -3$, and should therefore show the standard self-similar scaling. We did not however obtain an analytical expression analogous to (13) for its growth.

Figure 11 is a plot of $\log[k_c(a, \phi_c)]$ vs. a with $n = -2$, for 4 different values of ϕ_c . Also shown in the plot are the scalings expected from self-similarity, $k \propto a^{-2}$, and the scaling resulting from the solution for $\delta\phi$ given by equation (13), $k \propto a^{-1}$. This is the same as the velocity scaling referred to in Sections 2 and 3. The plots show that for $\phi_c = \pi$ and $\pi/2$, the velocity scaling is closely followed, typically to better than 20%; but for the lower values $\phi_c = \pi/4$ and $\pi/8$, self-similar scaling is more closely followed at the same level of accuracy. We verified that the trends did reflect a gradual transition in the scaling of $k_c(a, \phi_c)$ by plotting a larger range of ϕ_c down to $\phi_c = \pi/20$.

The dual scaling behavior shown by the phase shift can be interpreted as follows. For a given k , at early times as the phase just begins to depart from the linear solution (in which ϕ remains constant in time), its evolution is dominated by perturbative or other weakly nonlinear effects. These effects in general involve the coupling of a range of values of k' , mostly in the vicinity of $k' = k$, and obey the standard self-similar scaling. However at late times the phase shift is dominated by the bulk flow due to the longest waves in the box. The resulting phase change is given by equation (13) — it is a smooth function of a and k , and therefore dominates the more stochastic, dynamical components of the phase change at late times. Thus the phase shows behavior that we can interpret as arising from a combination of the kinematical divergence, and a dynamical, nonlinear component which obeys the standard self-similar scaling. The former drives $k_c(a, \phi_c)$ to the $k_c \propto a^{-1}$ scaling at late times, and the latter to the $k_c \propto a^{-2}$ scaling at early times.

Figure 13 shows $k_c(a, \phi_c)$ vs. a for the $n = 0$ spectrum. These results are from a P³M simulation performed by S. White, with 100^3 particles and $\epsilon = L/2500$. The $n = 0$ spectrum shows only one behavior, the self-similar scaling, $k \propto a^{-2/3}$. This is expected as the linear

bulk velocity does not diverge, therefore the longest waves in the box do not dominate the phase shift at any time.

For the amplitude scaling, Figure 12 shows a plot of $\log[k_c(a, \Delta_c)]$ vs. a with $n = -2$, for $\Delta_c = 0.25, 0.5, 1, 2$. For sufficiently high k , all four curves closely follow the standard self-similar scaling, $k \propto a^{-2}$, to better than 20% accuracy. This is consistent with the results for the power spectrum, as one would expect since the power spectrum measures the variance of the amplitude. All the curves show a departure from the $k \propto a^{-2}$ scaling at low k , for $k < 10$, with the discrepancy exceeding a factor of 2 in the amplitude. This most likely indicates that the absence of power on modes with wavelengths larger than the box-size has slowed the growth of modes which would otherwise be enhanced by coupling to modes longer than the box. Thus the standard self-similar solution for $n = -2$ is obtained only on scales significantly smaller than the box-size. For $n = 0$ the self-similar scaling $k \propto a^{-2/3}$ is again shown convincingly in Figure 14.

Our results are in partial disagreement with those of Gramann (1992). She found that for $n = -1$ in two dimensions (the analog of $n = -2$ in three dimensions), the standard self-similar scaling is broken for both the phase and amplitude. Our results for the phase scaling are consistent with hers, but the amplitude scalings are quite different: our results show good agreement with the scaling $k_c \propto a^{-2}$, whereas hers agree with $k_c \propto a^{-1}$. Since the statistics that we have measured are exactly the same as hers, it is difficult to explain the origin of the disagreement. It is conceivable that there are basic differences in the dynamics in two and three dimensions, but this is not reflected in the analytical results of Paper I. It is also possible that effects of the finite box-size are more prominent in two dimensions.

6. Conclusion

In Section 2 we summarized the motivation for examining the self-similar scaling of scale free spectra, $P(k) \propto k^n$, for $-3 < n < -1$. We have examined this issue through analytical techniques in Paper I and N-body techniques in this paper. In Paper I we found through two different approaches that the self-similar scaling of the amplitude of the density, and therefore of any measure of dynamical evolution, is preserved for $-3 < n < 1$.

In this paper we have tested the scaling of $n = -2$ scale free simulations. In Section 3 we discuss the issues of numerical resolution involved in such tests by comparing the resolution of three different simulations. We find that for the $n = -2$ spectrum we need the full resolution of our largest simulation, a P³M simulation with 256^3 particles to measure

its scaling properties. Section 4 shows that self-similar scaling is verified by the power spectrum measured from this simulation. Figures 4 and 5 demonstrate the existence of this scaling, and contrast it with an alternate scaling driven by the large-scale velocity field. We have compared our results with the recent work of Colombi, Bouchet & Hernquist (1995); Jain, Mo & White (1995); Lacey & Cole (1994); and Padmanabhan et al. (1995). We find that the shape of the nonlinear spectrum is well fit by the formulae proposed by Jain, Mo & White (1995) and Peacock & Dodds (1996), though the formulae slightly underestimate the spectrum in the strongly nonlinear regime. The shape of $P(k)$ at high- k agrees with the stable clustering prediction $P \propto k^{-2}$.

The second test of the scaling properties of the density field made in Section 5 relies on the mode-by-mode evolution of the amplitude and phase. At sufficiently late times the phase shift obeys the velocity scaling, consistent with the solution found in Paper I. At early times the evolution of the phase shift is consistent with the standard self-similar scaling. Thus the phase shift arises from a combination of kinematical effects due to large scale flows which dominate at late times, and genuine dynamical effects which dominate at relatively early times — in the weakly nonlinear stage of its evolution. The scaling of the amplitude follows the standard self-similar form, except at wavenumbers $k \lesssim 10$ (in units of $2\pi/L$) which we believe is a numerical limitation due to the finite size of the box. This is consistent with the analytical results of Paper I and with the results for the power spectrum.

In combination with the analytical analysis of Paper I, our results lead us to conclude with some confidence that the self-similar evolution of the density contrast is preserved for $-3 < n < -1$. The kinematical interpretation for the scaling of the phase shift provides a useful guide to identifying statistics susceptible to such effects. The rms displacement of particle positions is an example of a statistic which would be dominated by the bulk motions from long wave modes for $n < -1$, and must therefore be used with caution as a measure of nonlinear evolution.

We thank Simon White for providing the results of his scale free simulations, and for several useful suggestions. We also acknowledge useful discussions with Shep Doeleman, Mirt Gramann, Alan Guth, Ofer Lahav, Adi Nusser, Bepi Tormen and, especially, David Weinberg. This work was supported by NSF grant AST-9529154 and a grant of supercomputer time from the National Center for Supercomputing Applications. BJ acknowledges support from NASA through the LTSA grant NAG 5-3503.

REFERENCES

- Bertschinger, E. 1992, in *New Insights into the Universe*, ed. Martinez, V. J., Portilla, M. & Saez, D. (Berlin: Springer-Verlag), p. 65
- Bertschinger, E., & Gelb, J. 1991, *Comp. in Physics*, 5, 164
- Colombi, S., Bouchet, F., & Hernquist, L. 1996, *ApJ*, 465, 14
- Davis, M., & Peebles, P. J. E. 1977, *ApJS*, 34, 425
- Efstathiou, G. 1990, in *Physics of the Early Universe*, ed. Peacock, J. A., Heavens, A. F. & Davies, A. T. (Bristol: IOP), p. 361
- Efstathiou, G., & Eastwood, J. W. 1981, *MNRAS*, 194, 503
- Efstathiou, G., Davis, M., Frenk, C. S., & White, S. D. M., *ApJS*, 57, 241
- Efstathiou, G., Frenk, C. S., White, S. D. M., & Davis, M. 1988, *MNRAS*, 235, 715
- Ferrell, R. & Bertschinger, E. 1995, *Proceedings of the Society for Computer Simulation Multiconference*
- Ferrell, R. & Bertschinger, E. 1994, *International Journal of Modern Physics C*, 5, 933
- Gelb, J. M., & Bertschinger, E. 1994, *ApJ*, 436, 467
- Gramann, M. 1992, *ApJ*, 401, 19
- Jain, B., & Bertschinger, E. 1996, *ApJ*, 456, 43 (Paper I)
- Jain, B., Mo, H. J., & White, S. D. M. 1995, *MNRAS* 276, L25
- Klypin, A. A., & Melott, A. A. 1992, *ApJ*, 399, 397
- Lacey, C., & Cole, S. 1994, *MNRAS*, 272, 676
- Padmanabhan, T., Cen, R., Ostriker, J. P., & Summers, F. J. 1996, *ApJ*, 466, 604
- Peacock J.A., & Dodds S.J., 1994, *MNRAS*, 267, 1020
- Peacock J.A., & Dodds S.J., 1996, *MNRAS*, 280, L19
- Peebles, P. J. E. 1974, *A&A*, 32, 391

Peebles, P. J. E. 1980, *The Large-Scale Structure of the Universe* (Princeton: Princeton University Press)

Press, W. H., & Schechter, P. 1974, *ApJ*, 187, 425

Ryden, B. S., & Gramann, M. 1991, *ApJ*, 383, L33

Scherrer, R. J., Melott, A. L., & Shandarin, S. F. 1991, *ApJ*, 377, 29

Splinter, R. J., Melott, A. L., & Shandarin, S. F. 1997, *astro-ph/9711105*

Suginohara, T., & Suto, Y. 1991, *ApJ*, 371, 470

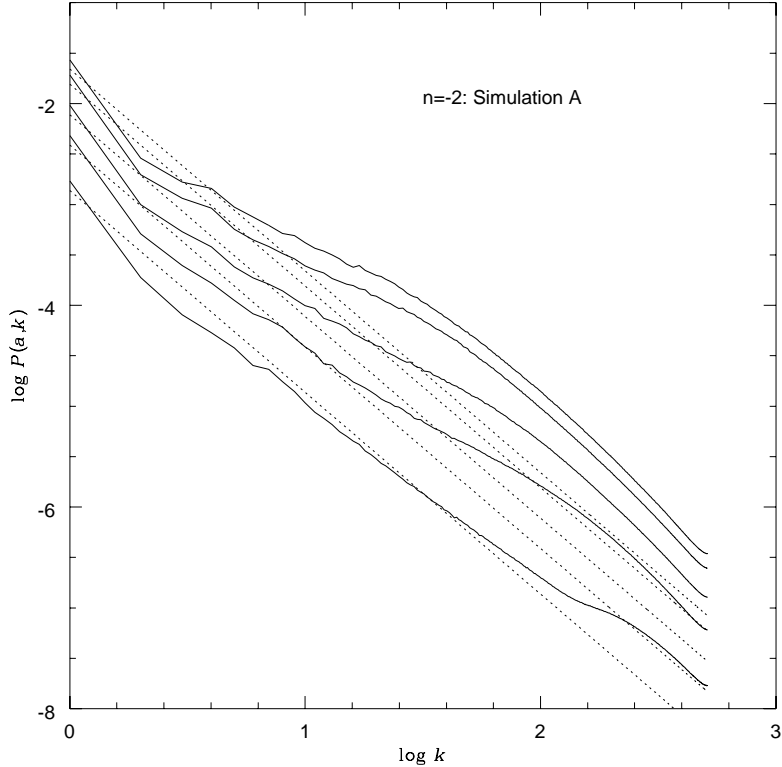


Fig. 1.— The power spectrum $P(k)$ vs. k measured from simulation A at five different times. The solid curves show the N-body power spectrum for $k_{nl}(a) = 58, 29, 14.5, 7.25$. The wavenumber k is in units of $2\pi/L$. The dotted lines show the linear spectrum $P \propto a^2 k^{-2}$ at the same times. The N-body spectrum at low- k shows statistical fluctuations due to the small number of modes available to measure it. At high- k the spectrum is plotted up to $1/2$ the Nyquist frequency of the FFT grid, $k = 512$.

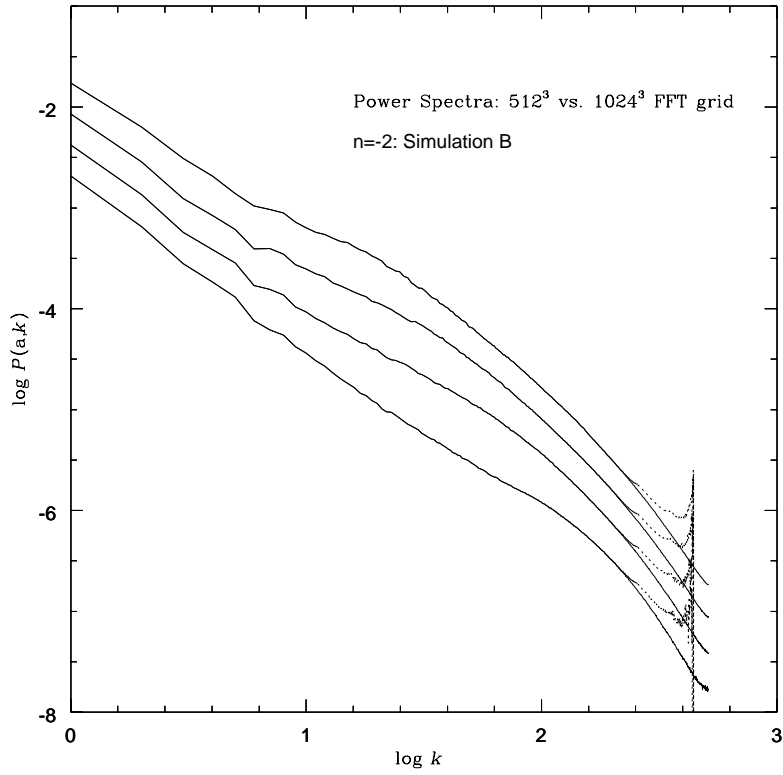


Fig. 2.— The effect of the FFT grid on $P(k)$ at high- k . The two solid curves show the power spectrum computed from simulation B with different grid sizes: 512^3 and 1024^3 . The spectrum measured with a 512^3 grid is plotted with a dotted curve between $k = 257 - 512$, to show the artificial features introduced by the grid used to interpolate the real space density.

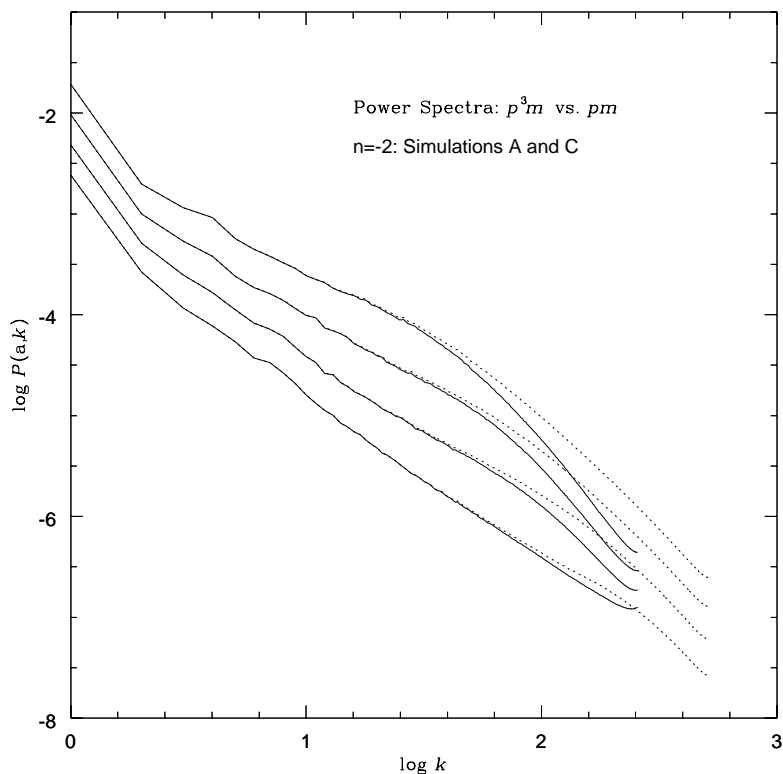


Fig. 3.— The effect of limited resolution on the power spectrum. The solid curves show the power spectrum measured from simulation C, a PM simulation with the same number of particles as simulation A, a P^3M simulation. The spectra are computed on a 512^3 grid and are shown at the same output times as those of Figure 1. The dotted curves show the spectra from simulation A, computed using a 1024^3 grid. Both spectra are plotted up to $1/2$ the Nyquist frequency of the FFT grid. A comparison of the two sets of spectra shows that as time evolves, the power in the PM simulation is suppressed on an increasingly large range of k .

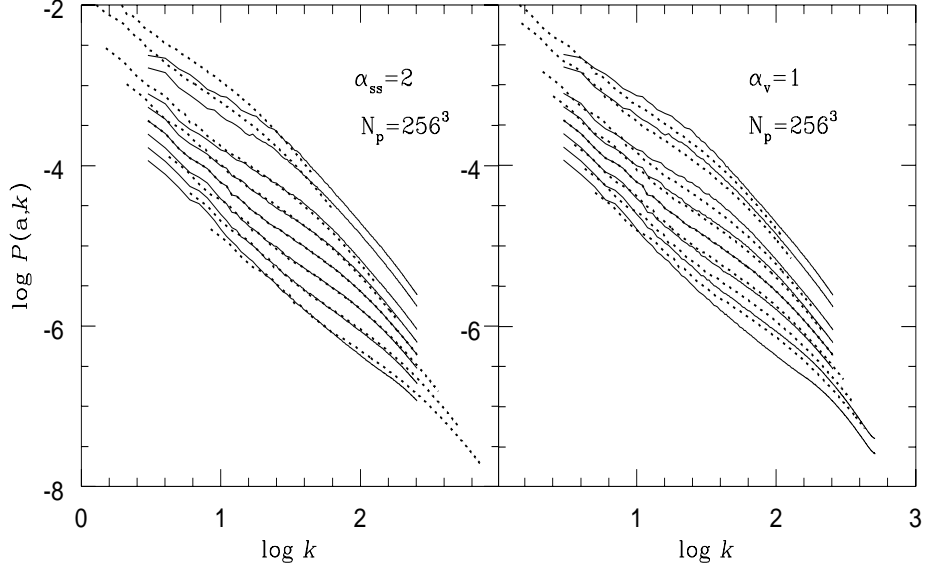


Fig. 4.— The scaling of the power spectrum for the $n = -2$ simulation A. Simulation A is a P^3M simulation with 256^3 particles. The solid curves show the N-body power spectrum at eight different output times spanning $k_{nl}(a) = 58 - 7.25$. The dotted curves are all obtained by scaling the spectrum at the fourth from last output time: the wavenumber is scaled as $k \propto a(\tau)^{-\alpha}$, and the spectrum is scaled to maintain consistency with the linear spectrum. The left panel shows the results for the standard self-similar scaling with $\alpha = 2$. The dotted curves agree very well with the solid curves except at the smallest and largest k owing to the finite resolution of the simulation. The right panel shows the velocity scaling with $\alpha = 1$.

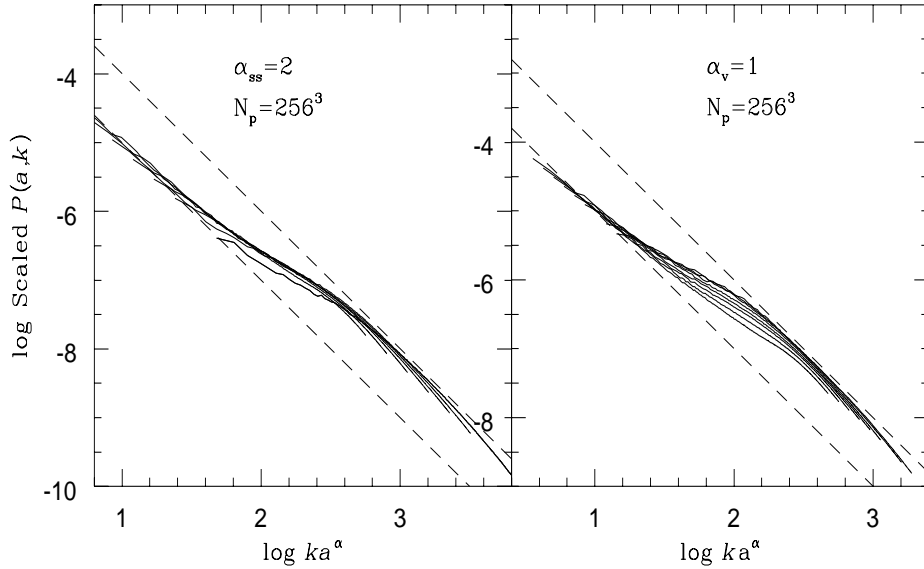


Fig. 5.— The same power spectra as in Figure 4 are shown, but the scaling is tested a little differently. The power spectra and wavenumbers at the eight output times are scaled so that they would all lie along a single curve if the scaling were correct. Again the standard self-similar scaling shown in the left panel works better than the alternate velocity scaling shown in the right panel. The lower dashed line shows the linear spectrum. The upper dashed line has arbitrary amplitude, but its slope is predicted by the stable clustering hypothesis. The N-body spectra asymptote to this slope at high- k .

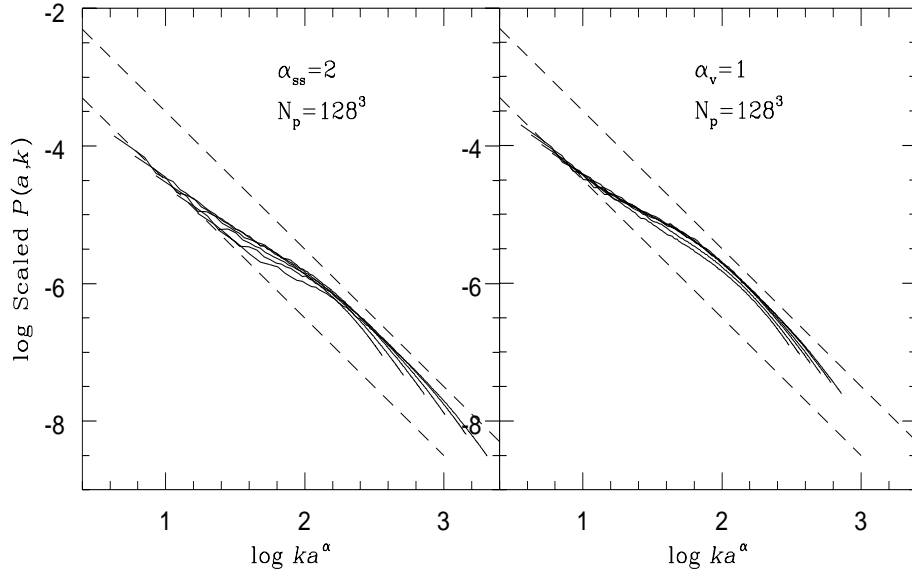


Figure 6

Fig. 6.— This is identical to Figure 5, but for simulation B which has 128^3 particles and twice as large a spatial resolution as simulation A. The results shown in the two panels are not able to distinguish the different scalings. This figure demonstrates the need for larger simulations, like the one shown in Figures 4 and 5, to effectively test the scaling properties of the $n = -2$ spectrum.

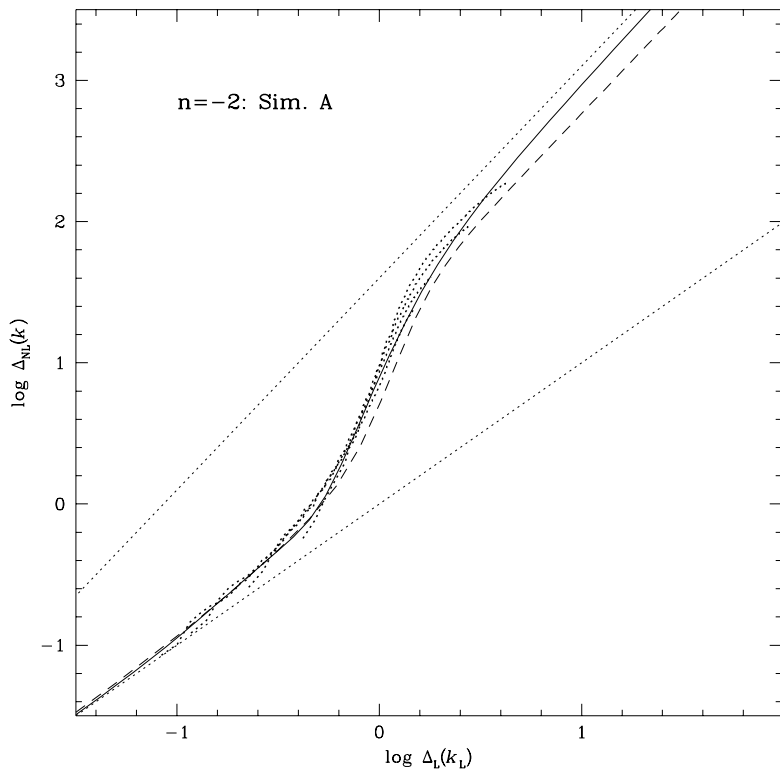


Fig. 7.— Comparison of N-body spectra with analytical fitting formulae. The dotted curves show the dimensionless power $\Delta(k) = 4\pi k^3 P(k)$ plotted against the linear power on wavenumber k_L , as described in Section 4.1. The curves are obtained from the N-body spectrum of simulation A at the same times as in Figure 1. The solid curve is the fitting formula of Jain, Mo & White (1995) as given in equation (10) and the dashed curve is from the fitting formula of Peacock & Dodds (1996). The upper dotted line shows the slope predicted by the stable clustering hypothesis, while the lower dotted line is the linear theory relation.

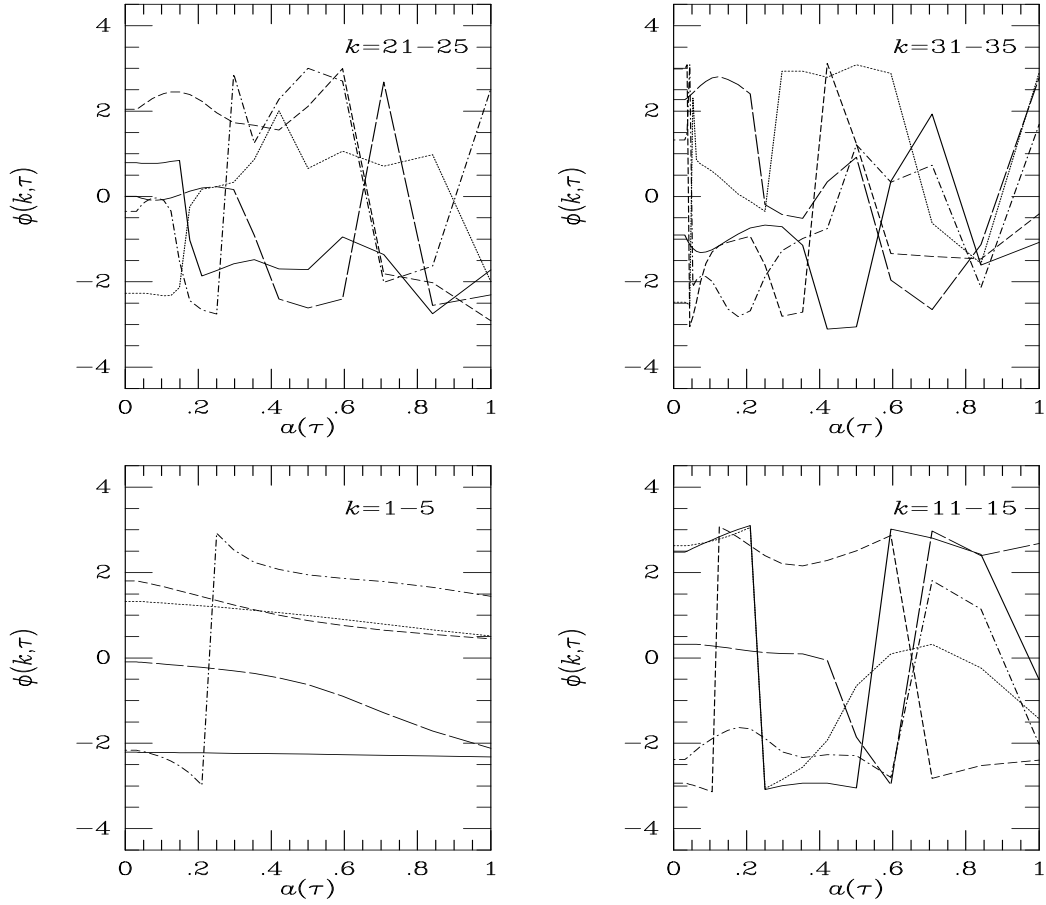


Fig. 8.— Phase trajectories for the $n = -2$ simulation B. The trajectories of the phases $\phi(\vec{k}, \tau)$ of individual Fourier modes for $n = -2$ are plotted vs. $a(\tau)$. The magnitudes k of the wavevectors are labeled in each panel; the full vectors were chosen as $\vec{k} = (0, 0, k)$. Within each panel k increases in the following order: solid, dotted, dashed, long-dashed, dashed-dotted curves. The phase is defined modulo 2π , and is therefore constrained to lie between $-\pi$ and π . At $a = 0$, the value of ϕ at the earliest time has been plotted again to show the expected linear behavior.

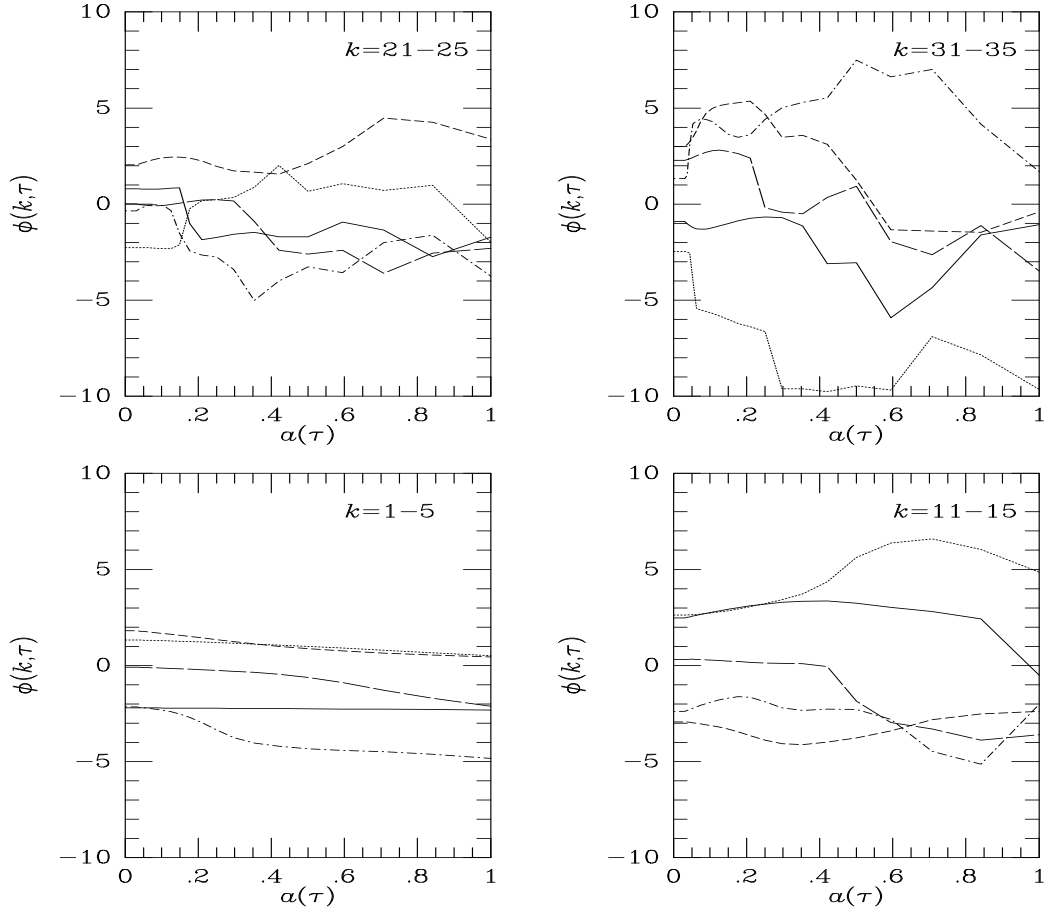


Fig. 9.— “Re-defined” phase trajectories for $n = -2$. The same trajectories as in Figure 8 are plotted, but ϕ has been re-defined so that it is no longer constrained between $-\pi$ and π (notice the limits on the y-axis), as described in Section 5.1. In linear theory the phases do not change with time; significant departures from this can be seen in all but the lowest k modes.

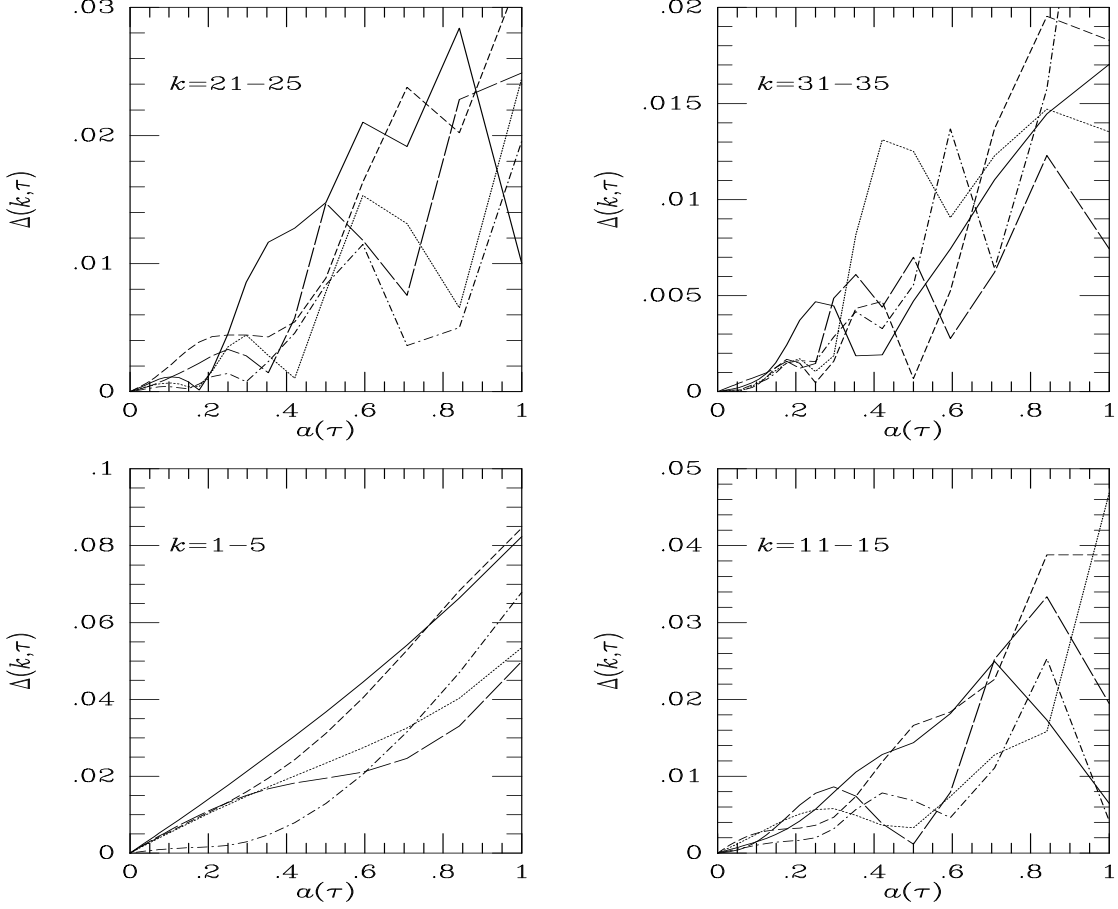


Fig. 10.— Amplitude trajectories for $n = -2$. The trajectories of the amplitudes $\Delta(\vec{k}, \tau)$ of individual Fourier modes for $n = -2$ are plotted vs. a , as in Figure 9 for the phase. Note that at early times $\Delta \propto a$: to check this all the curves have been joined to $\Delta = 0$ at $a = 0$. Therefore the lowest value of a at which departures from a straight line occur shows nonlinear behavior.

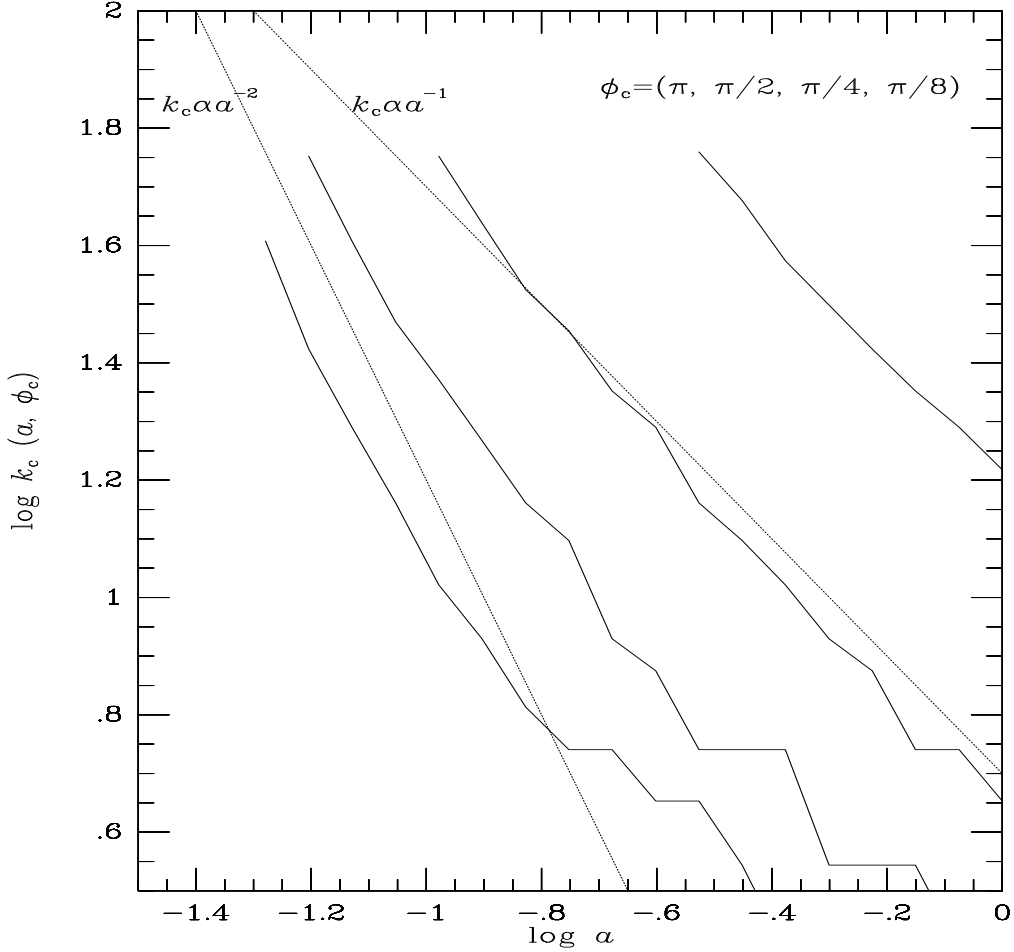


Fig. 11.— Characteristic scales from the phase for $n = -2$. The scaling of characteristic wavenumber scales, k_c vs. a is shown, as derived from the mean phase deviation. $k_c(a, \phi_c)$ is the value of k at which $\langle |\delta\phi(\vec{k}, a)| \rangle = \phi_c$. The four solid curves correspond to the values of ϕ_c labeled at the top of the plot. Note that for high values of ϕ_c (the top 2 curves), the scaling closely agrees with $k_c \propto a^{-1}$, shown by the upper dotted line. A transition towards the standard self-similar scaling $k_c \propto a^{-2}$, shown by the lower dotted line, occurs for the two lower values of ϕ_c .

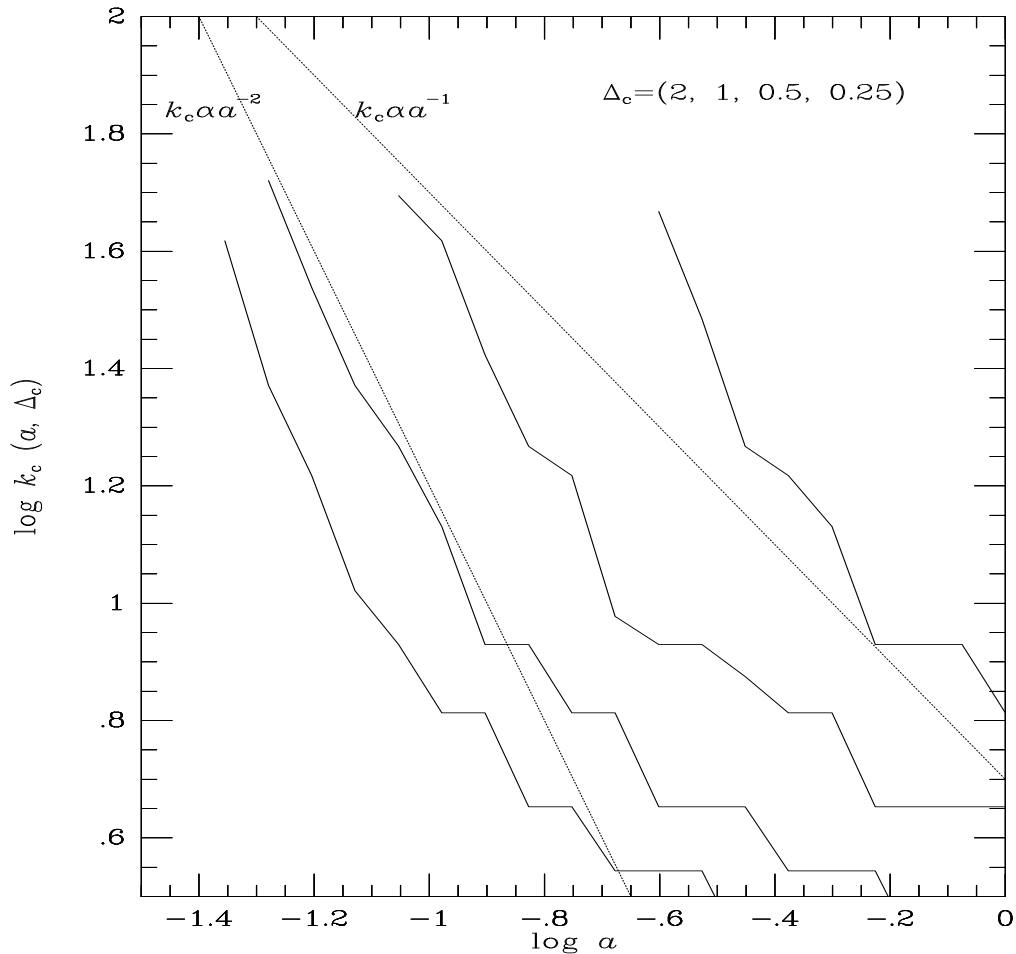


Fig. 12.— Characteristic scales from the amplitude for $n = -2$. The scaling of characteristic wavenumber scales derived from the departure of the amplitude from linear growth, $k_c(a, \Delta_c)$ vs. a is shown for 4 different values of Δ_c (see equation (12) for the definition of $k_c(a, \Delta_c)$). All the curves have a slope close to the standard self-similar scaling, $k_c \propto a^{-2}$ at high k . For k below about 10 the slope becomes shallower, probably due to the limitation of a finite box.

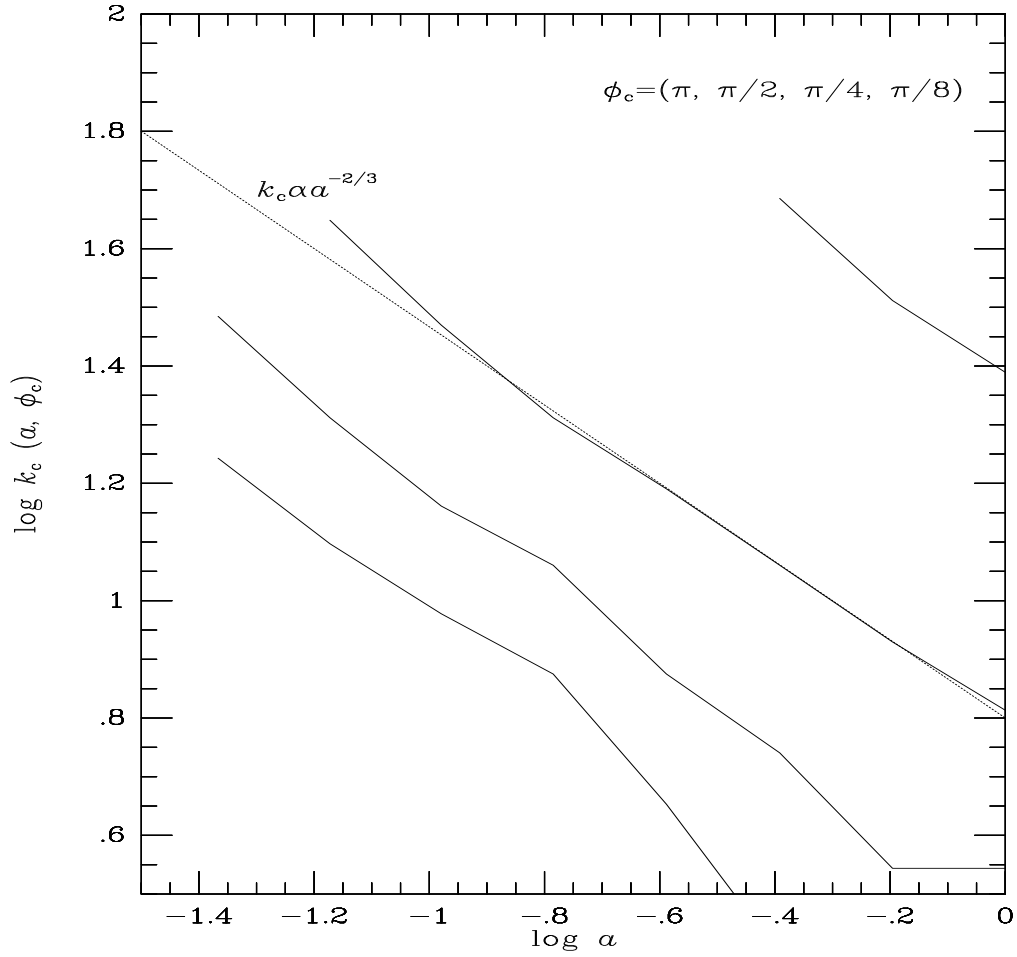


Fig. 13.— Characteristic scales from the phase for $n = 0$. For $n = 0$ the scaling k_c vs. a is shown using the mean phase deviation. Notice that in contrast to the $n = -2$ case, here only one behavior for all values of ϕ_c is evident: the self-similar scaling $k_c \propto a^{-2/3}$.

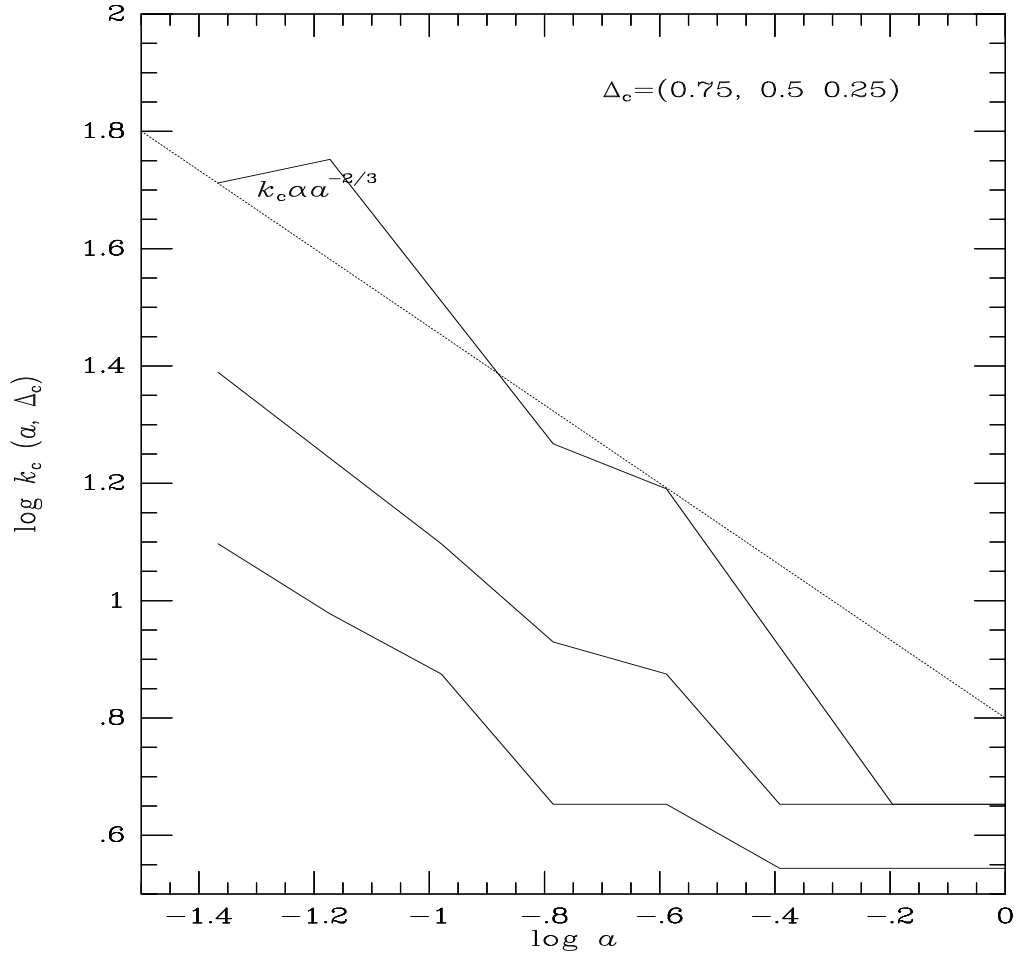


Fig. 14.— Characteristic scales from the amplitude for $n = 0$. For $n = 0$ the scaling k_c vs. a is shown using the mean amplitude. Again, as in Figure 13, the standard self-similar scaling is recovered.